Environmental Science & Technology

pubs.acs.org/est

Open Access

This article is licensed under CC-BY 4.0

Article

Redox-Driven Formation of Mn(III) in Ice

Tao Chen, Tra My Bui Thi, Tao Luo, Wei Cheng, Khalil Hanna, and Jean-François Boily*

Cite This: *Environ. Sci. Technol.* 2024, 58, 15194−15201

Read Online

ACCESS | Metrics & More | Article Recommendations | Supporting Information

ABSTRACT: Redox-driven reactions involving Mn(II) species adsorbed at Mn(IV) oxide surfaces can release Mn(III) in the form of dissolved Mn(III)−ligand species in natural waters. Using pyrophosphate (PP) as a model ligand, we show that freezing accelerates and enhances Mn(III) formation in the form of Mn(III)−PP complexes. This freeze-promoted reaction is explained by the concentration of Mn(IV) oxides and solutes (Mn(II), Na^+, and Cl^-) into the minute fractions of liquid water locked between ice (micro)crystals - the Liquid Intergrain Boundary (LIB). Time-resolved freezing experiments at −20 °C showed that Mn(III) yields were greatest at low salt (NaCl) content. In contrast, high salt content promoted Mn(III) formation through chloride complexation, although yields became lower as the cryosalt mineral hydrohalite ($NaCl{\cdot}2H_2O$) dehydrated the LIB by drawing water into its structure. Consecutive freeze−thaw cycles also showed that dissolved Mn(III) concentrations increased within the very first few minutes of each freezing event. Because each thaw event released unreacted PP previously locked in ice, each sequential freeze−thaw cycle increased Mn(III) yields, until ∼80% of the Mn was converted to Mn(III). This was achieved after only seven cycles. Finally, temperature-resolved freezing experiments down to −50 °C showed that the LIB produced the greatest quantities of Mn(III) at −10 °C, where the volumes were greater. Reactivity was however sustained in ice formed below the eutectic (−21.3 °C), down to −50 °C. We suspect that this sustained reactivity was driven by persistent forms of supercooled water, such as Mn(IV) oxide-bound thin water films. By demonstrating the freeze-driven production of Mn(III) by comproportionation of dissolved Mn(II) and Mn(IV) oxide, this study highlights the potentially important roles these reactions could play in the production of pools of Mn(III) in natural water and sediments of mid- and high-latitudes environments exposed to freeze−thaw episodes.

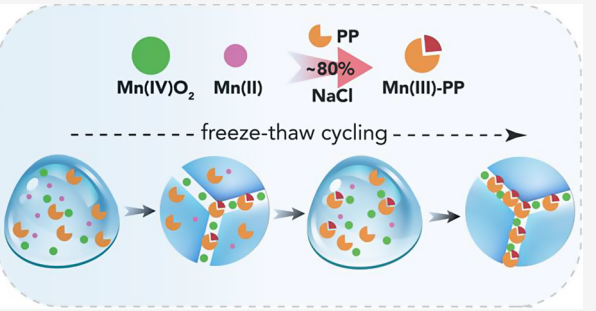

KEYWORDS: *ice, manganese, biogeochemical cycle, redox*

Downloaded via UMEA UNIV on September 16, 2024 at 09:20:39 (UTC).
See https://pubs.acs.org/sharingguidelines for options on how to legitimately share published articles.

1. INTRODUCTION

Manganese (Mn) is the third most abundant-redox active[1] metal in Earth's crust,[2] and is of great importance to many redox-driven biogeochemical processes.[3] In natural aquatic systems, Mn(II), Mn(III), and Mn(IV) species are present over a wide range of environmental redox conditions, and undergo rapid cycling between these states.[4] Mn(IV) forms strongly oxidizing minerals (e.g., cryptomelane (α-MnO_2), pyrolusite (β-MnO_2), and birnessite (δ-MnO_2)),[5] while Mn(II) is primarily in the form of dissolved aqueous species.[6,7] Mn can also form minerals, such as rhodochrosite ($MnCO_3$), in reducing environments.[8]

Interactions between Mn(II) species and Mn(IV) oxides have been the focus of many studies following Mn(II)-induced heavy metal sorption[9−12] and phase transformation[13−15] reactions. Mn(III) species have, on the other hand, not received as much attention given their strong propensity to disproportionate into Mn(IV) oxides and Mn(II) species, and for precipitating into oxyhydroxides (e.g., feitknechtite (β-Mn(III)OOH), Manganite (γ-Mn(III)OOH)) or mixed valent Mn(III, IV) oxides (e.g., hausmannite (Mn_3O_4)).[13−16] Still, Mn(III) can form stable aqueous species under acidic conditions and, under circumneutral conditions, as (in)-organically complexed species.[17−20]

In nature, soluble Mn(III) can be released by the abiotic and biotic oxidation of Mn(II)[3,21−24] or by the reduction of MnO_2.[25,26] This can take place through a one electron transfer reaction,[27] as well as through ligand-promoted nonreductive[28,29] and reductive dissolution[5,30−32] of Mn-bearing minerals. The potentially important roles that Mn(III) species play in nature can be attributed to their prolonged lifetime when bound to (in)organic ligands (L). These Mn(III)−L species can, as a result, secure Mn(III) transport across redox gradients in nature.[7,33,34] For instance, Mn(III)−L complexes represent the majority of the total dissolved Mn(III) pool in anoxic, suboxic and oxic environments of oceanic and estuarian sediments, where they can be present up to tens of micromolar

Received: April 18, 2024
Revised: August 13, 2024
Accepted: August 13, 2024
Published: August 17, 2024

© 2024 The Authors. Published by American Chemical Society

level.[19,35,36] Mn(III)−L species also account for the great majority of dissolved Mn species in suboxic waters of the Black[19] and Baltic[37] seas, and 90% of soluble Mn in sediment porewaters of the Laurentian Trough.[33] Soluble Mn(III) was even detected at every stage in a water treatment work in England, particularly when Mn oxide solids interacted with natural organic matter in the clarifier sludge.[38]

Although the composition of complexing ligands is still not well-known, compounds responsible for stabilizing Mn(III) include naturally occurring carboxylate- or phosphonate-bearing moieties in natural ligands.[17] These ligands include organic chelates, for instance natural organic matter (e.g., humic substances),[39] ethylenediaminetetraacetate (EDTA),[40] citrate,[30] and siderophores (e.g., desferrioxamine B),[41] as well as polyphosphates.[17,29,42,43] These ligands, especially polyphosphates, are likely important contributors to Mn cycling in nature.[33] The reactive Mn(III), serving as both electron donor and acceptor, may even possibly be linked to the cycling of carbon, arsenic, iron, and sulfur.[44,45]

The natural occurrence of soluble Mn(III) could, however, be altered in frozen environments of the Cryosphere. This chemistry is driven by minute fractions of liquid water locked between ice microcrystals in polycrystalline ice formed above the eutectic temperature of NaCl-bearing water (−21.3 °C). Particulate matter and solutes concentrated into this Liquid Intergrain Boundary (LIB) can react at different rates and generate different products than in liquid water.[46−51] This could, as such, be the case for the important comproportionation reactions that control Mn redox geochemistry. Evaluating the role that freezing could play on geochemical reactions is particularly relevant noting that about two-thirds of Earth's entire freshwater supply is stored in ice and glaciers, and that a great portion of the water in mid- to high-latitude regions can freeze or even undergo several freeze−thaw episodes during cold seasons.[52]

In this study, we addressed the roles that freezing plays in the formation of Mn(III) by reacting dissolved Mn(II) and birnessite (MnO_2), an important nanolayered Mn(IV)-oxide nanomineral. Both commonly occur in water columns and sediments at concentrations of tens of microns.[19,53] We used pyrophosphate (PP) as redox-inert chelating ligand to stabilize Mn(III) in the form of aqueous Mn(III)−pyrophosphate (Mn(III)−PP) complexes.[42] The focus on PP was also motivated by its presence in aquatic environments, such as in marine particulate and estuary sediments and even in industrial discharge, present in the order of tens to hundreds of micromoles.[36,54−56] By exploring how temperature, ionic strength, pH, and freeze−thaw cycling affected Mn comproportionation reactions in the LIB, we showed that freezing greatly enhances reaction rates and yields of Mn(III) species. These findings should contribute to understanding Mn cycling as species migrate through interconnected bodies of water in the cryosphere and the hydrosphere, including those from fresh to oceanic waters.

2. EXPERIMENTAL METHODS

2.1. Solutions and Materials. Stock solutions of manganese(II) chloride tetrahydrate, and sodium pyrophosphate decahydrate salts (Sigma-Aldrich) were prepared in ultrapure water. Manganese(III) acetate dihydrate (Sigma-Aldrich) was used as received without purification. Standard solutions of premade 1 M NaOH or 1 M HCl (Sigma-Aldrich) were used to adjust the pH of the solutions. Acid birnessite was synthesized by reacting $KMnO_4$ and HCl in boiling water.[57] The resulting suspension was purged from dissolved atmospheric CO_2(g) using a stream of N_2(g), then stored in the dark at 4 °C. The study of Li et al.[57] contains a detailed report on the synthesis and purification procedures, as well as salient physicochemical properties of the high specific surface area (85 m^2/g) MnO_2 nanoparticles used for this work.

2.2. Batch Experiments. Batch experiments were conducted in transparent polyethylene centrifuge tubes containing 10 mL of pH ∼ 7 solutions of 250 μM pyrophosphate and 50 μM $MnCl_2$ solutions in 0−50 mM NaCl. The theoretical PP:Mn(III) = 2.5:1 ratio, assuming full conversion of Mn, chosen for this work ensured that all Mn(III) species can in most cases be complexed with PP at circumneutral pH,[42] as confirmed by thermodynamic calculations of the aqueous solutions using the program PHREEQC (Figure S4, Table S2).[58]

Reactions were initiated by adding a 50 μM MnO_2(s) to the solution. The resulting suspensions (4.35 mg/L MnO_2(s)) were immediately shaken manually, each sealed with a septum. Based on control experiments in the dark at 25 °C, the low MnO_2 suspension densities used in this work were not sufficiently large to initially alter suspension pH. Samples were thereafter frozen to −10, −20, −30, or −50 ± 0.1 °C by submerging the test tubes into precooled liquid ethanol in a circulation bath. Samples were completely frozen within ∼2 min. From the uniform distribution of color along the tubes of the frozen samples, we infer that MnO_2 particles were well-dispersed throughout the frozen suspensions. Frozen samples were then periodically withdrawn from the ethanol bath and thawed in lukewarm water (30−40 °C) for ∼5 min. This thawing period was not sufficiently long to react Mn(III) species any further, as we could assess by comparing reaction yields in liquid water. The resulting aqueous suspensions were then filtered (0.2 μm filter) and the supernatant analyzed for Mn(III).

Freeze−thaw (F−T) cycling experiments were performed in the same fashion as the freezing experiments, except that they consisted of 45 min cycles, each comprising a period of 20 min in liquid water (25 °C), followed by another 20 min period in ice (−20 °C), and a final ∼5 min thawing period in lukewarm water. Two sets of freeze−thaw cycling experiments were performed. One set of experiments in 0.5 mM NaCl was carried out for 7 consecutive cycles. Another set of experiments at 12 different ionic strengths within the 0.5−500 mM NaCl range, were analyzed for Mn(III) after 1, 3, and 7 F−T cycles.

All batch freezing experiments were performed in the dark without controlling the atmosphere of the headspace, unless otherwise noted. Contributions from oxygen-driven formation of Mn(III) were negligible, as additional sets of experiments showed no difference in Mn(III) content in samples reacted under aerobic and anaerobic conditions (Figure S1). All experiments were repeated at least twice, and with a reproducibility of ∼5% in Mn(III) concentrations.

2.3. Mn(III) Concentration Determination. Concentrations of Mn(III)−PP complexes were measured by UV−vis spectrophotometry. From the aqueous speciation of mixed Mn(III)/PP solutions (Figure S4, Table S2), Mn(III) should be predominantly in the form of the $MnPP_2^{5-}$ complex. A 10 mM Mn(III) and 40 mM PP stock solution used to prepare standards was made by adding a weighed aliquot of dry manganese(III) acetate dihydrate powder to a 40 mM sodium pyrophosphate decahydrate solution at pH ∼ 8.[29,40,42] The

https://doi.org/10.1021/acs.est.4c03850
Environ. Sci. Technol. 2024, 58, 15194−15201

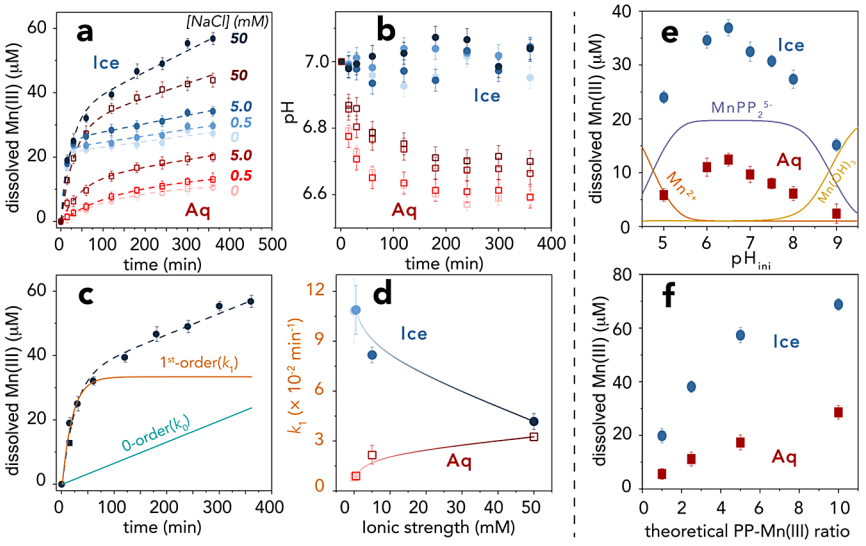

Figure 1. Mn(III) formation by comproportionation of 50 μM MnO_2 (4.35 mg/L) and 50 μM Mn^{2+} in the presence of (a–d) 250 μM PP at pH_{ini} = 7 ± 0.05, and variations in Mn(III) concentrations versus (e) pH and (f) theoretical PP-Mn(III) ratio. All reactions in liquid water (Aq) were at 25 °C and in ice (Ice) at −20 °C. (a) Time-resolved Mn(III) concentrations (symbols) and kinetic models (dashed lines), (b) changes in pH in 0–50 mM NaCl, (c) detailed kinetic modeling in frozen 50 mM NaCl, and (d) first-order rate constants (symbols) with lines as a visual guide. (e) pH-dependent Mn(III) concentrations after 2 h of reaction in 0.5 mM NaCl against chemical speciation at equilibrium (Figure S4, Table S2). (f) PP:Mn(III) ratio dependence on Mn(III) after 2 h of reaction in 0.5 mM NaCl as a function of "theoretical PP-Mn(III) ratio" (i.e., full conversion of 50 μM Mn(IV) and 50 μM Mn(II) to 100 μM Mn(III)).

solution was equilibrated with magnetic stirrer, and the pH shifted to ∼7. The resulting standard solution was then stored in the dark in a refrigerator at 4 °C to mitigate PP decomposition. The experimental work was completed well within any significant decomposition of the standard Mn(III)–PP solutions, which have a half-life of several hundreds of days.[40,42]

The UV–vis spectra of all Mn(III)–PP standards and analytes were collected in the 200–800 nm range in a 10 mm quartz cell using an ultraviolet–visible (UV–vis) spectrophotometer (Cary-50, Varian). All absorbances were offset to 0 in the 600–800 nm range to correct minor shifts in absorbances. Mn(III) concentrations were then determined using absorbance values at 258 nm (linear fit of calibration curve with r^2 > 0.99). Note that absorbances were not affected by pH, given a previous report on the molar absorbances for Mn(III)–PP complexes.[40]

2.4. Mn(II) Adsorption on MnO_2. Mn(II) adsorption experiments were conducted in 10 mL test tubes containing 50 μM $MnCl_2$ and 50 μM MnO_2(s) (4.35 mg/L) in the presence and absence of 250 μM PP in 0.5 mM NaCl at pH 7. Experiments were carried out at 25 and −20 °C for 1 h. Those at −20 °C were followed by a ∼5 min period of thawing in lukewarm water. All resulting aqueous suspensions were thereafter filtered (0.2 μm) and analyzed for dissolved Mn using inductively coupled plasma-atomic emission spectrometry (ICP-AES, 725-ES, Varian).

Changes in surface Mn oxidation state on reacted MnO_2(s) were probed by X-ray photoelectron spectroscopy (XPS). Solids collected from batch adsorption experiments were first washed with N_2(g)-sparged Milli-Q water (18.2 MΩ·cm) to remove residual dissolved Mn and pyrophosphate, then dried under a stream of N_2(g). Spectra of the resulting dry solids were thereafter acquired using a Kratos Axis Ultra electron spectrometer equipped with monochromatic Al K_α X-ray (1486.7 eV) source operating at 10 mA and 15 kV. Mn oxidation states were evaluated by spectral fitting of the Mn $2p_{3/2}$ region using the approach of Ilton et al.[59] Briefly, the procedure involves a combination of Gaussian/Lorentzian (G/L) peaks (Figure S6) obtained from solid-state references (Table S3) for Mn(II) ($MnCl_2$), Mn(III) (MnOOH; Manganite), and Mn(IV) (MnO_2; pyrolusite).[59,60] All fitting procedures were performed on CasaXPS,[61] using a Shirley background on all spectra.

2.5. Raman Spectroscopy. The cryosalt mineral hydrohalite ($NaCl·2H_2O$) formed by freezing NaCl-bearing solutions was probed by Raman spectroscopy. Spectra were acquired with a Renishaw InVie Qontor Raman spectrometer using a 532 nm continuous wave laser with a 50× Long Working Distance Objective Lens. Measurements were performed on single ∼10 μL droplets of 0.5–500 mM NaCl solutions dropped on a temperature-controlling microscope stage (Linkam Scientific THMS600). Temperature was then decreased from 25 to −20 °C at a rate of 5 °C/min using liquid nitrogen as the cooling agent. The microscope was then focused on the surface of the frozen droplet, and an optical image was obtained to identify the spatial distribution of the LIBs. Spectra were thereafter collected in the O–H stretching region (2600–4000 cm^{-1}), with a total of 100 scans with the objective refocused on selected portions of LIBs.

3. RESULTS AND DISCUSSIONS

Time-resolved batch experiments (Figure 1a) showed that comproportionation reactions in ice (−20 °C) were ∼10 times faster and produced ∼2.5 times more Mn(III) than those in liquid water (25 °C) after 6 h of reaction. Also, from the unchanged values of pH ∼ 7, losses in proton concentration from the reactions (e.g., $Mn^{2+} + MnO_2(s) + 4H^+ \rightarrow 2\ Mn^{3+} + 2H_2O$) were smaller than the buffering capacity of the system. In contrast, a shift in the pH from ∼6.8 to ∼6.6 in the unfrozen samples may have resulted from the progressive uptake of atmospheric CO_2. This shift was, however, not sufficient to

https://doi.org/10.1021/acs.est.4c03850
Environ. Sci. Technol. 2024, 58, 15194–15201

significantly alter aqueous speciation, as evaluated by thermodynamics. (Figures S3 and S4).

Mn(III) concentrations produced in liquid water scaled with ionic strength (Figure 1a). This can be well described using a zero- and first-order composite model (Figure 1c, Table S1):

$$[\mathrm{Mn(III)} - \mathrm{PP}] = [\mathrm{Mn(III)} - \mathrm{PP}]_{\infty}(1 - e^{-k_1 t}) + k_0 t \quad (1)$$

where $[\mathrm{Mn(III)}-\mathrm{PP}]_{\infty}$ is the concentration of Mn(III)−PP at equilibrium, k_1 is the first-order reaction rate constant, and k_0 is the zero-order reaction rate constant. Contributions from the ligand-assisted dissolution of Mn(III) from MnO_2 or abiotic oxidation of Mn^{2+} were ruled out (Figure S1). We ascribe (i) k_1 to fast Mn^{2+} adsorption reactions with negatively charged MnO_2 sites (point of zero charge, $pH_{pzc} \sim 2$) in the stages of the reaction,[29,57] and (ii) k_0 to slower adsorption reaction on neutrally charged basal faces of MnO_2 and potentially to diffusion to interlayer sites.[62] Both rates scaled in liquid water with ionic strength (Figures 1d and S2), and this is supported by studies[63−65] showing that Mn-chloride complexation facilitates electron transfer rates. In contrast, first-order Mn(III) formation rates (k_1) in ice were ∼10 times larger than in liquid water at low ionic strength, yet nearly identical at 50 mM NaCl (Figure 1d). We attribute this enhancement at low ionic strengths to the locking of reactive species (MnO_2, Mn^{2+} and PP) in the LIB after freezing. This locking caused first-order reactions to dominate in the first ∼40 min of freezing, initially producing ∼20 to 30 μM Mn(III) (Figure 1a).

To explain these results, we explored (i) Mn speciation using thermodynamic calculations (Figures S3 and S4, Table S2), as well as (ii) Mn(III) yields as a function of pH (Figure 1e) and Mn:PP ratios (Figure 1f). We make the following three key observations:

(i) From thermodynamics, we note that the main reactive species should be the free Mn^{2+} (42%) and the complexed $MnPP^{2-}$ (58%) ions (Figure S3). The Mn^{2+} ion should consequently be the main adsorbing Mn species, given the low pH_{pzc} of the Mn(IV) oxide. From batch adsorption experiments (Figure S5), we find that these reactions began with an initial loading of ∼20 Mn/nm^2. Mn(III) formed in both liquid water and ice via one-electron interfacial transfer of the adsorbed Mn^{2+} complexes to MnO_2. This was confirmed by XPS (Figure 2), showing a substantial comproportionation of Mn(II) (6.0 → 0.0%) and Mn(IV) (61.4 → 14.3%) to Mn(III) (32.6 → 85.7%) in the absence of PP (Figures 2a,b), and that Mn(II):Mn(III):Mn(IV) remained relative unchanged during the ligand-assisted dissolution of the newly formed surface Mn(III) species by PP (Figure 2c,d). The following reactions:

$$MnO_2 + Mn^{2+} + 2H_2O \rightarrow 2MnOOH + 2H^+ \quad (2)$$

$$MnOOH + HPP^{3-} + H_2PP^{2-} \rightarrow MnPP_2^{5-} + 2H_2O \quad (3)$$

explain speciation and oxidation changes undergone in the system.

(ii) Second, experiments showed that the largest concentrations of Mn(III) after 2 h were at pH 6−7 (Figure 1e). Smaller concentrations of Mn(III) produced at low and high pH can be explained by freeze-induced shifts in pH. More extreme pH converted $MnPP_2^{5-}$ to hydrolyzable PP species (Figure S4). We expect that these shifts occurred because

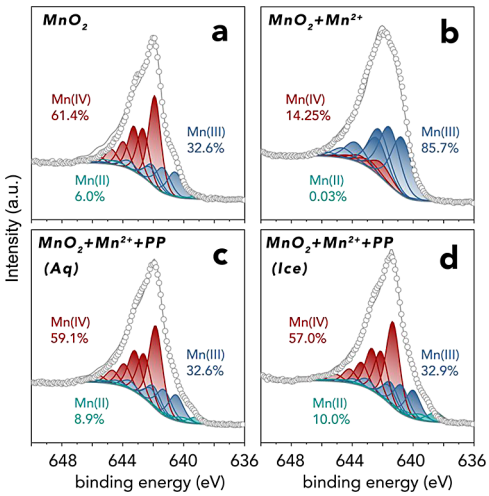

Figure 2. XPS spectra and fitting results of the Mn $2p_{3/2}$ region of (a) unreacted MnO_2, (b) MnO_2 reacted with Mn^{2+} in the absence of PP in liquid water at 25 °C, and (c-d) MnO_2 reacted with Mn^{2+} and PP in (c) liquid water (Aq) at 25 °C and (d) in ice at −20 °C (Ice). Atomic % values of Mn oxidation states are shown for every sample.

excess H^+ or OH^- ions in noncircumneutral solutions migrated to or from the LIB during freezing. These shifts could have also been accentuated by the differential partitioning of solute between ice and water,[66,67] and even by the spontaneous disproportionation of Mn(III) below pH ∼ 5 ($E_H^0{}_{(Mn3+/Mn2+)}$ = +1.56 V)[68].

(iii) Third, we found that Mn(III) concentrations scaled with PP:Mn(III) ratios (Figure 1f). A PP:Mn(III) ratio of 2 was needed to convert Mn(III) to $MnPP_2^{5-}$ (Figure S4), and even higher ratio (PP:Mn(III) > 5) is usually required to fully stabilize Mn(III) at circumneutral pH.[42] Previous work[29] however showed that PP, just like other ligands,[69] can promote Mn detachment from MnO_2.

These results therefore support the concept that the freeze-driven concentration of PP into the LIB catalyzed Mn(III) production by both mitigating disproportionation[63] and buffering pH. This was even the case at a PP:Mn(III) ratio of 1:1, where the freeze concentration effect increased PP:Mn(III) ratios to levels that generated ∼4 times more Mn(III) in ice than in liquid water. This Mn(III)-promoting freeze concentration effect became, however, less effective at larger PP dosages. One possible explanation for this nonlinear response to PP dosage could be that a fraction of unreacted PP species was trapped in ice. This explanation aligns with previous work[70] showing that solids and selected solutes tend to be mostly rejected from ice crystals, while other ligands can also be readily incorporated into the ice lattice.[70]

To test this idea of reagent trapping by ice, we tracked Mn(III) formation through a sequence of 7 freeze−thaw (F−T) cycles. These experiments (Figure 3a) revealed that each freeze event produced progressively more Mn(III) until the seventh F−T cycle, where concentrations plateaued at ∼80 μM Mn(III). This amounts to ∼8 times more Mn(III) than in liquid water at 25 °C (∼10 μM, Figure 1a), and to ∼80% of the Mn in the system. These systematic hikes in Mn(III) concentration align with those seen in the ∼40 min of freezing in the time-resolved experiments (Figure 1a). They can thus be most readily explained by reaction of species that were previously trapped in ice, and subsequently released during thawing events. This interpretation aligns with one of the very

https://doi.org/10.1021/acs.est.4c03850
Environ. Sci. Technol. 2024, 58, 15194−15201

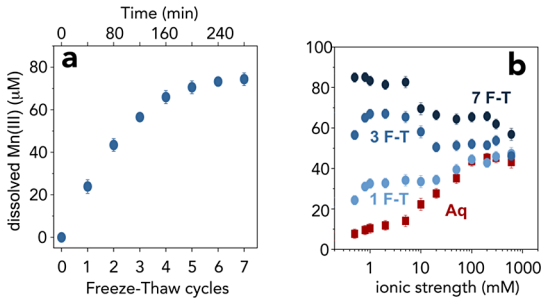

Figure 3. Mn(III) formation by freeze−thaw (F−T) cycling of pH_{ini} = 7 ± 0.05 suspensions of 50 μM MnO_2 (4.35 mg/L), 50 μM Mn^{2+} and 250 μM PP in (a) 0.5 mM NaCl and (b) 0.5−500 mM NaCl. Each 40 min cycle comprised a 20 min period of reaction in liquid water (25 °C) followed by a 20 min period in frozen water (−20 °C).

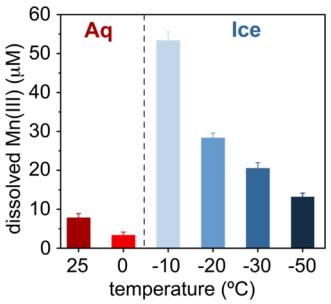

Figure 4. Temperature effects on dissolved Mn(III) production in liquid water (Aq) and ice (Ice). Mn(III) produced in 2 h of reaction by comproportionation of 50 μM MnO_2 (4.35 mg/L) and 50 μM Mn^{2+} in the presence of 250 μM PP in solutions of 0.5 mM NaCl at pH_{ini} = 7 ± 0.05.

few other published studies on heterogeneous cryo-redox reactions,[71] which showed that F−T cycling promoted the oxidative transformation of iodine by Fe(III) into reactive iodine, and of this iodine converted to organoiodine when reacted with natural organic matter.

To explore the salt-dependence on the freezing-driven formation of Mn(III), we performed an additional set of F−T experiments covering the 0.5−500 mM NaCl range (Figure 3b). We focused on results after the 1st, 3rd and 7th F−T cycles (Figure 3a). These experiments revealed that freezing enhanced Mn(III) formation at up to ∼50 mM NaCl after 1 F−T cycle, and at all NaCl concentrations after 3 and 7 F−T cycles. Additionally, while Mn(III) yields scaled with NaCl content after 1 F−T cycle, those obtained after 3 and 7 F−T cycles were smaller the higher the NaCl content. Still they were consistently higher than in liquid water.

We explain these results by the competing effects of (i) chloride-promoted redox reactions,[63−65] and (ii) the salt-dependent availability of liquid water in the LIB. Chloride-promoted reactions, which can clearly be appreciated in liquid water, were best manifested in ice after 1 F−T cycle. Here, freezing promoted Mn(III) formation by increasing the chloride content in the LIB, where the reactions took place. This freeze concentration effect was most effective in dilute NaCl because relative changes in LIB NaCl concentrations were greatest.[51] As a result, this effect became attenuated at high salt content, chiefly explaining the identical yields after 1 F−T cycle and those achieved in liquid water. Compounded on this effect, is the loss of LIB liquid water by the formation of the cryosalt mineral hydrohalite ($NaCl{\cdot}2H_2O$), whose growth withdraws liquid water from the LIB.[72] We can support this claim using Raman microscopy (Figure S7) showing that hydrohalite formed in the LIB at the higher salt content. This salt-driven removal of water from the LIB can thus explains the smaller Mn(III) yields at this ionic strength, and as especially observed after 3 and 7 F−T cycles.

In an effort to test how temperature and availability impact Mn(III) formation, we compared Mn(III) yields in warm (25 °C) and cold (∼0 °C) liquid water, then in ice at the temperatures crossing the eutectic (−21.3 °C), down to −50 °C (Figure 4). These experiments confirmed again the strong enhancement of Mn(III) generated in ice in relation to liquid water. The strongest yields were at −10 °C, where liquid water coexisted with ice.[73] Again, we attribute this enhancement to the accumulation of reactive MnO_2, Mn^{2+} and PP in the LIB. While this notion for a sustained activity of ice below the eutectic clashes with the classical idea that reactivity should have been suppressed,[51] earlier[74,75] and an increasingly growing body of evidence[76−78] are lending support to the idea that small persistent populations of liquid water can be preserved in the form of (i) supercooled intergrain boundary water[73,79] resulting from the freezing process, and (ii) quasi-liquid layers at surfaces of ice microcrystals and MnO_2 particles.[80,81] These are certainly avenues worthy of investigation in forthcoming studies, and which can lead to new ideas of geochemical reactions at extremely low temperatures.

4. ENVIRONMENTAL IMPLICATIONS

We showed that freezing greatly accelerated the formation of dissolved Mn(III)−PP complexes from the comproportionation between solid MnO_2 and dissolved Mn(II) species. Freeze concentration of reactants in the LIB of ice was proposed to be the main driving force for Mn(III) formation. Seven consecutive freeze−thaw cycles led to the conversion of up to ∼80% of all Mn into Mn(III) species at low ionic strengths. Conversion at high ionic strength was, in contrast, not at high but promoted by Cl complexation.[63−65]

This study on the impact of freezing on dissolved Mn(III) formation revealed that freezing can be an important formation pathway contributing to natural pools of soluble Mn(III) in nature. Although this work focused on comproportionation reactions in the presence of only pyrophosphate, our findings can be generalized to other Mn(III)-stabilizing (in)organic ligands. In particular, these can include natural organic matter, which possesses Mn(III)-complexing chelating functional groups.

Our findings may consequently imply that soluble Mn(III) aquatic and estuary settings in middle- to high-latitude regions could be catalyzed by freeze−thaw episodes. This idea could potentially help explain recently reported high fluxes of dissolved Mn in creeks and estuaries during Spring snowmelt events.[82] It could also help understand the coupled biogeochemical cycling of Mn with those of carbon, nitrogen, sulfur, oxygen, and iron.[33,44,45] Recognition of the impact of freezing on the biogeochemical cycling of Mn may even shed new light on these cycles, especially that the dynamics of the hydrosphere and cryosphere are increasingly altered by climate change.

https://doi.org/10.1021/acs.est.4c03850
Environ. Sci. Technol. 2024, 58, 15194−15201

■ ASSOCIATED CONTENT

Supporting Information

The Supporting Information is available free of charge at https://pubs.acs.org/doi/10.1021/acs.est.4c03850.

Time profile of Mn(III) formation in ligand-assisted dissolution of MnO_2 or abiotic oxidation of Mn^{2+}; ionic strength-dependence on zero-order rate constants; aqueous speciation of Mn^{2+} and PP over pH; distribution of dissolved Mn species after reactions in liquid water and ice; XPS spectra of reference Mn-phases; Raman microscopy image and spectra of ice microcrystals and the LIB; kinetic model parameters; and thermodynamic constants for the aqueous Mn and PP species (PDF)

■ AUTHOR INFORMATION

Corresponding Author

Jean-François Boily − *Department of Chemistry, Umeå University, SE-901 87 Umeå, Sweden;* orcid.org/0000-0003-4954-6461; Email: jean-francois.boily@umu.se

Authors

Tao Chen − *École Nationale Supérieure de Chimie de Rennes, CNRS, ISCR-UMR 6226, Université de Rennes, F-35000 Rennes, France;* orcid.org/0000-0002-8238-4823

Tra My Bui Thi − *École Nationale Supérieure de Chimie de Rennes, CNRS, ISCR-UMR 6226, Université de Rennes, F-35000 Rennes, France;* orcid.org/0000-0001-8839-8428

Tao Luo − *École Nationale Supérieure de Chimie de Rennes, CNRS, ISCR-UMR 6226, Université de Rennes, F-35000 Rennes, France*

Wei Cheng − *College of Resources and Environmental Science, South-Central University for Nationalities, Wuhan 430074, P. R. China*

Khalil Hanna − *École Nationale Supérieure de Chimie de Rennes, CNRS, ISCR-UMR 6226, Université de Rennes, F-35000 Rennes, France;* orcid.org/0000-0002-6072-1294

Complete contact information is available at: https://pubs.acs.org/10.1021/acs.est.4c03850

Notes

The authors declare no competing financial interest.

■ ACKNOWLEDGMENTS

The authors wish to thank support from Swedish Research Council (2020-04853), FORMAS (2022-01246) and Carl-Tryggers (CTS 22:2326) to J.F.B., the French National Research Agency via the INFLOW project (ANR-21-CE29-0008-01) to K.H., the CNRS (IRP CHEMICY 2022-2027) to K.H. and J.F.B., and a China Scholarship Council for a Ph.D. grant and Région Bretagne for a mobility grant for an extended research stay at Umeå University to T.C.

■ REFERENCES

(1) Zhang, S.; Livi, K. J. T.; Gaillot, A. C.; Stone, A. T.; Veblen, D. R. Determination of Manganese Valence States in (Mn^{3+}, Mn^{4+}) Minerals by Electron Energy-Loss Spectroscopy. *Am. Mineral.* **2010**, *95* (11−12), 1741−1746.

(2) Butterfield, C. N.; Soldatova, A. V.; Lee, S. W.; Spiro, T. G.; Tebo, B. M. Mn(II,III) Oxidation and MnO_2 Mineralization by an Expressed Bacterial Multicopper Oxidase. *Proc. Natl. Acad. Sci. U. S. A.* **2013**, *110* (29), 11731−11735.

(3) Powell, M. J. D. A Method for Minimizing a Sum of Squares of Non-Linear Functions Without Calculating Derivatives. *Comput. J.* **1965**, *7* (4), 303−307.

(4) Johnson, K. S. Manganese Redox Chemistry Revisited. *Science.* **2006**, *313*, 1896−1897.

(5) Stone, A. T.; Morgan, J. J. Reduction and Dissolution of Manganese(III) and Manganese(IV) Oxides by Organics: 2. Survey of the Reactivity of Organics. *Environ. Sci. Technol.* **1984**, *18* (8), 617−624.

(6) Tipping, E.; Thompson, D. W.; Davison, W. Oxidation Products of Mn(II) in Lake Waters. *Chem. Geol.* **1984**, *44* (4), 359−383.

(7) Soldatova, A. V.; Romano, C. A.; Tao, L.; Stich, T. A.; Casey, W. H.; Britt, R. D.; Tebo, B. M.; Spiro, T. G. Mn(II) Oxidation by the Multicopper Oxidase Complex Mnx: A Coordinated Two-Stage Mn(II)/(III) and Mn(III)/(IV) Mechanism. *J. Am. Chem. Soc.* **2017**, *139* (33), 11381−11391.

(8) Tan Luong, N.; Ilton, E. S.; Shchukarev, A.; Boily, J. F. Water Film-Driven Mn (Oxy)(Hydr)Oxide Nanocoating Growth on Rhodochrosite. *Geochim. Cosmochim. Acta* **2022**, *329*, 87−105.

(9) Wu, Y.; Li, W.; Sparks, D. L. The Effects of Iron(II) on the Kinetics of Arsenic Oxidation and Sorption on Manganese Oxides. *J. Colloid Interface Sci.* **2015**, *457*, 319−328.

(10) Lefkowitz, J. P.; Elzinga, E. J. Impacts of Aqueous Mn(II) on the Sorption of Zn(II) by Hexagonal Birnessite. *Environ. Sci. Technol.* **2015**, *49* (8), 4886−4893.

(11) Zhao, H.; Feng, X.; Lee, S.; Reinhart, B.; Elzinga, E. J. Sorption and Oxidation of Co(II) at the Surface of Birnessite: Impacts of Aqueous Mn(II). *Chem. Geol.* **2023**, *618*, No. 121281.

(12) Lefkowitz, J. P.; Elzinga, E. J. Structural Alteration of Hexagonal Birnessite by Aqueous Mn(II): Impacts on Ni(II) Sorption. *Chem. Geol.* **2017**, *466*, 524−532.

(13) Elzinga, E. J. Reductive Transformation of Birnessite by Aqueous Mn(II). *Environ. Sci. Technol.* **2011**, *45* (15), 6366−6372.

(14) Lefkowitz, J. P.; Rouff, A. A.; Elzinga, E. J. Influence of pH on the Reductive Transformation of Birnessite by Aqueous Mn(II). *Environ. Sci. Technol.* **2013**, *47* (18), 10364−10371.

(15) Zhao, H.; Zhu, M.; Li, W.; Elzinga, E. J.; Villalobos, M.; Liu, F.; Zhang, J.; Feng, X.; Sparks, D. L. Redox Reactions between Mn(II) and Hexagonal Birnessite Change Its Layer Symmetry. *Environ. Sci. Technol.* **2016**, *50* (4), 1750−1758.

(16) Ramstedt, M.; Sjöberg, S. Phase Transformations and Proton Promoted Dissolution of Hydrous Manganite (γ-MnOOH). *Aquat. Geochemistry* **2005**, *11* (4), 413−431.

(17) Wang, Y.; Stone, A. T. Phosphonate- and Carboxylate-Based Chelating Agents That Solubilize (Hydr)Oxide-Bound MnIII. *Environ. Sci. Technol.* **2008**, *42* (12), 4397−4403.

(18) Liu, J.; Zhang, Y.; Gu, Q.; Sheng, A.; Zhang, B. Tunable Mn Oxidation State and Redox Potential of Birnessite Coexisting with Aqueous Mn(II) in Mildly Acidic Environments. *Minerals* **2020**, *10* (8), 690.

(19) Trouwborst, R. E.; Clement, B. G.; Tebo, B. M.; Glazer, B. T.; Luther, G. W. Soluble Mn(III) in Suboxic Zones. *Science* **2006**, *313* (5795), 1955−1957.

(20) Davies, G. Some Aspects of the Chemistry of Manganese(III) in Aqueous Solution. *Coord. Chem. Rev.* **1969**, *4* (2), 199−224.

(21) Liu, J.; Inoué, S.; Zhu, R.; He, H.; Hochella, M. F. Facet-Specific Oxidation of Mn(II) and Heterogeneous Growth of Manganese (Oxyhydr)Oxides on Hematite Nanoparticles. *Geochim. Cosmochim. Acta* **2021**, *307*, 151−167.

(22) Han, X.; Li, Y. L.; Gu, J. D. Abiotic Oxidation of Mn(II) and Its Effect on the Oxidation of As(III) in the Presence of Nano-Hematite. *Ecotoxicology* **2012**, *21* (6), 1753−1760.

(23) Davies, S. H. R.; Morgan, J. J. Manganese(II) Oxidation Kinetics on Metal Oxide Surfaces. *J. Colloid Interface Sci.* **1989**, *129* (1), 63−77.

(24) Cerrato, J. M.; Falkinham, J. O.; Dietrich, A. M.; Knocke, W. R.; McKinney, C. W.; Pruden, A. Manganese-Oxidizing and -Reducing Microorganisms Isolated from Biofilms in Chlorinated Drinking Water Systems. *Water Res.* **2010**, *44* (13), 3935−3945.

(25) Huang, J.; Zhong, S.; Dai, Y.; Liu, C. C.; Zhang, H. Effect of MnO_2 Phase Structure on the Oxidative Reactivity toward Bisphenol A Degradation. *Environ. Sci. Technol.* **2018**, *52* (19), 11309−11318.
(26) Allard, S.; von Gunten, U.; Sahli, E.; Nicolau, R.; Gallard, H. Oxidation of Iodide and Iodine on Birnessite (δ-MnO_2) in the pH Range 4−8. *Water Res.* **2009**, *43* (14), 3417−3426.
(27) Luther, G. W. Manganese(II) Oxidation and Mn(IV) Reduction in the Environment - Two One-Electron Transfer Steps versus a Single Two-Electron Step. *Geomicrobiol. J.* **2005**, *22* (3−4), 195−203.
(28) Klewicki, J. K.; Morgan, J. J. Dissolution of β-MnOOH Particles by Ligands: Pyrophosphate, Ethylenediaminetetraacetate, and Citrate. *Geochim. Cosmochim. Acta* **1999**, *63* (19−20), 3017−3024.
(29) Liu, W.; Sun, B.; Qiao, J.; Guan, X. Influence of Pyrophosphate on the Generation of Soluble Mn(III) from Reactions Involving Mn Oxides and Mn(VII). *Environ. Sci. Technol.* **2019**, *53* (17), 10227−10235.
(30) Flynn, E. D.; Catalano, J. G. Reductive Transformations of Layered Manganese Oxides by Small Organic Acids and the Fate of Trace Metals. *Geochim. Cosmochim. Acta* **2019**, *250*, 149−172.
(31) Xyla, A. G.; Sulzberger, B.; Luther, G. W.; Hering, J. G.; Van Cappellen, P.; Stumm, W. Reductive Dissolution of Manganese-(III,IV) (Hydr)Oxides by Oxalate: The Effect of pH and Light. *Langmuir* **1992**, *8* (1), 95−103.
(32) Ritschel, T.; Totsche, K. U. Reductive Transformation of Birnessite by Low-Molecular-Weight Organic Acids. *Chemosphere* **2023**, *325*, No. 138414.
(33) Madison, A. S.; Tebo, B. M.; Mucci, A.; Sundby, B.; Luther, G. W. Abundant Porewater Mn(III) Is a Major Component of the Sedimentary Redox System. *Science* **2013**, *341* (6148), 875−878.
(34) Soldatova, A. V.; Tao, L.; Romano, C. A.; Stich, T. A.; Casey, W. H.; Britt, R. D.; Tebo, B. M.; Spiro, T. G. Mn(II) Oxidation by the Multicopper Oxidase Complex Mnx: A Binuclear Activation Mechanism. *J. Am. Chem. Soc.* **2017**, *139* (33), 11369−11380.
(35) Jones, M. R.; Luther, G. W.; Tebo, B. M. Distribution and Concentration of Soluble Manganese(II), Soluble Reactive Mn(III)-L, and Particulate MnO_2 in the Northwest Atlantic Ocean. *Mar. Chem.* **2020**, *226*, No. 103858.
(36) Oldham, V. E.; Owings, S. M.; Jones, M. R.; Tebo, B. M.; Luther, G. W. Evidence for the Presence of Strong Mn(III)-Binding Ligands in the Water Column of the Chesapeake Bay. *Mar. Chem.* **2015**, *171*, 58−66.
(37) Dellwig, O.; Schnetger, B.; Brumsack, H. J.; Grossart, H. P.; Umlauf, L. Dissolved Reactive Manganese at Pelagic Redoxclines (Part II): Hydrodynamic Conditions for Accumulation. *J. Mar. Syst.* **2012**, *90* (1), 31−41.
(38) Johnson, K. L.; McCann, C. M.; Wilkinson, J. L.; Jones, M.; Tebo, B. M.; West, M.; Elgy, C.; Clarke, C. E.; Gowdy, C.; Hudson-Edwards, K. A. Dissolved Mn(III) in Water Treatment Works: Prevalence and Significance. *Water Res.* **2018**, *140* (Iii), 181−190.
(39) Li, Q.; Xie, L.; Jiang, Y.; Fortner, J. D.; Yu, K.; Liao, P.; Liu, C. Formation and Stability of NOM-Mn(III) Colloids in Aquatic Environments. *Water Res.* **2019**, *149*, 190−201.
(40) Klewicki, J. K.; Morgan, J. J. Kinetic Behavior of Mn(III) Complexes of Pyrophosphate, EDTA, and Citrate. *Environ. Sci. Technol.* **1998**, *32* (19), 2916−2922.
(41) Duckworth, O. W.; Sposito, G. Siderophore-Manganese (III) Interactions. I. Air-Oxidation of Manganese(II) Promoted by Desferrioxamine B. *Environ. Sci. Technol.* **2005**, *39* (16), 6037−6044.
(42) Qian, A.; Zhang, W.; Shi, C.; Pan, C.; Giammar, D. E.; Yuan, S.; Zhang, H.; Wang, Z. Geochemical Stability of Dissolved Mn(III) in the Presence of Pyrophosphate as a Model Ligand: Complexation and Disproportionation. *Environ. Sci. Technol.* **2019**, *53* (10), 5768−5777.
(43) Kostka, J. E.; Luther, G. W.; Nealson, K. H. Chemical and Biological Reduction of Mn (III)-Pyrophosphate Complexes: Potential Importance of Dissolved Mn (III) as an Environmental Oxidant. *Geochim. Cosmochim. Acta* **1995**, *59* (5), 885−894.
(44) Wang, X.; Shu, Z.; He, H.; Zhou, M.; Lu, X.; Wang, J.; Zhang, L.; Pan, Z.; Wang, Z. Arsenopyrite Dissolution in Circumneutral Oxic Environments: The Effect of Pyrophosphate and Dissolved Mn(III). *Water Res.* **2023**, *230*, No. 119595.
(45) Wang, X.; Wang, J.; Lu, X.; Zhou, M.; Wang, Q.; Pan, Z.; Kumar, N.; Zhu, M.; Wang, Z. Oxidative Dissolution of Orpiment and Realgar Induced by Dissolved and Solid Mn(III) Species. *Geochim. Cosmochim. Acta* **2022**, *332*, 307−326.
(46) O'Concubhair, R.; O'Sullivan, D.; Sodeau, J. R. Dark Oxidation of Dissolved Gaseous Mercury in Polar Ice Mimics. *Environ. Sci. Technol.* **2012**, *46* (9), 4829−4836.
(47) Kvlividze, V. I.; Kiselev, V. F.; Kurzaev, A. B.; Ushakova, L. A. The Mobile Water Phase on Ice Surfaces. *Surf. Sci.* **1974**, *44* (1), 60−68.
(48) Anzo, K.; Harada, M.; Okada, T. Enhanced Kinetics of Pseudo First-Order Hydrolysis in Liquid Phase Coexistent with Ice. *J. Phys. Chem. A* **2013**, *117* (41), 10619−10625.
(49) Jeong, D.; Kim, K.; Min, D. W.; Choi, W. Freezing-Enhanced Dissolution of Iron Oxides: Effects of Inorganic Acid Anions. *Environ. Sci. Technol.* **2015**, *49* (21), 12816−12822.
(50) Gross, G. W.; Wong, P. M.; Humes, K. Concentration Dependent Solute Redistribution at the Ice-Water Phase Boundary. III. Spontaneous Convection. Chloride Solutions. *J. Chem. Phys.* **1977**, *67* (11), 5264−5274.
(51) Takenaka, N.; Bandow, H. Chemical Kinetics of Reactions in the Unfrozen Solution of Ice. *J. Phys. Chem. A* **2007**, *111* (36), 8780−8786.
(52) Khilchevskyi, V.; Karamushka, V. Global Water Resources: Distribution and Demand. In *Clean Water and Sanitation*; Leal Filho, W.; Azul, A. M.; Brandli, L.; Lange Salvia, A.; Wall, T., Eds.; Springer International Publishing: Cham, 2020; pp 1−11.
(53) Oldham, V. E.; Mucci, A.; Tebo, B. M.; Luther, G. W. Soluble Mn(III)−L Complexes Are Abundant in Oxygenated Waters and Stabilized by Humic Ligands. *Geochim. Cosmochim. Acta* **2017**, *199*, 238−246.
(54) Zhang, X.; Yang, Y.; Lv, X.; Wang, Y.; Liu, N.; Chen, D.; Cui, L. Adsorption/Desorption Kinetics and Breakthrough of Gaseous Toluene for Modified Microporous-Mesoporous UiO-66 Metal Organic Framework. *J. Hazard. Mater.* **2019**, *366*, 140−150.
(55) Jones, M. R.; Luther, G. W.; Mucci, A.; Tebo, B. M. Concentrations of Reactive Mn(III)-L and MnO_2 in Estuarine and Marine Waters Determined Using Spectrophotometry and the Leuco Base, Leucoberbelin Blue. *Talanta* **2019**, *200*, 91−99.
(56) Sundareshwar, P. V.; Morris, J. T.; Pellechia, P. J.; Cohen, H. J.; Porter, D. E.; Jones, B. C. Occurrence and Ecological Implications of Pyrophosphate in Estuaries. *Limnol. Oceanogr.* **2001**, *46* (6), 1570−1577.
(57) Li, Q.; Schild, D.; Pasturel, M.; Lützenkirchen, J.; Hanna, K. Alteration of Birnessite Reactivity in Dynamic Anoxic/Oxic Environments. *J. Hazard. Mater.* **2022**, *433*, No. 128739.
(58) Lu, P.; Zhang, G.; Apps, J.; Zhu, C. Comparison of Thermodynamic Data Files for PHREEQC. *Earth-Science Rev.* **2022**, *225*, No. 103888.
(59) Ilton, E. S.; Post, J. E.; Heaney, P. J.; Ling, F. T.; Kerisit, S. N. XPS Determination of Mn Oxidation States in Mn (Hydr)Oxides. *Appl. Surf. Sci.* **2016**, *366*, 475−485.
(60) Wang, X.; Wang, Q.; Yang, P.; Wang, X.; Zhang, L.; Feng, X.; Zhu, M.; Wang, Z. Oxidation of Mn(III) Species by Pb(IV) Oxide as a Surrogate Oxidant in Aquatic Systems. *Environ. Sci. Technol.* **2020**, *54* (21), 14124−14133.
(61) Fairley, N.; Fernandez, V.; Richard-Plouet, M.; Guillot-Deudon, C.; Walton, J.; Smith, E.; Flahaut, D.; Greiner, M.; Biesinger, M.; Tougaard, S.; Morgan, D.; Baltrusaitis, J. Systematic and Collaborative Approach to Problem Solving Using X-Ray Photoelectron Spectroscopy. *Appl. Surf. Sci. Adv.* **2021**, *5*, No. 100112.
(62) Li, Y.; Zhao, X.; Wu, J.; Gu, X. Surface Complexation Modeling of Divalent Metal Cation Adsorption on Birnessite. *Chem. Geol.* **2020**, *551*, No. 119774.
(63) Pan, J.; Gao, B.; Duan, P.; Guo, K.; Akram, M.; Xu, X.; Yue, Q.; Gao, Y. Improving Peroxymonosulfate Activation by Copper Ion-Saturated Adsorbent-Based Single Atom Catalysts for the Degradation

of Organic Contaminants: Electron-Transfer Mechanism and the Key Role of Cu Single Atoms. *J. Mater. Chem. A* **2021**, *9* (19), 11604−11613.
(64) Xu, F.; Ouyang, D. L.; Rene, E. R.; Ng, H. Y.; Guo, L. L.; Zhu, Y. J.; Zhou, L. L.; Yuan, Q.; Miao, M. S.; Wang, Q.; Kong, Q. Electricity Production Enhancement in a Constructed Wetland-Microbial Fuel Cell System for Treating Saline Wastewater. *Bioresour. Technol.* **2019**, *288*, No. 121462.
(65) Cheng, L.; Mao, Y.; Jiang, L.; Ma, R.; Ma, J.; Zhuo, Y.; Shen, Q.; Liu, C.; Zhao, L.; Xu, X.; Ji, F. Mn(VII) Enhanced by $CaSO_3$ to Remove Trace Organic Pollutants in High Salt Organic Wastewater: Further Enhancement of Salinity. *Chemosphere* **2023**, *334* (174), No. 138964.
(66) Watanabe, H.; Otsuka, T.; Harada, M.; Okada, T. Imbalance between Anion and Cation Distribution at Ice Interface with Liquid Phase in Frozen Electrolyte as Evaluated by Fluorometric Measurements of pH. *J. Phys. Chem. C* **2014**, *118* (29), 15723−15731.
(67) Kataoka, S.; Harada, M.; Okada, T. pH-Buffering Capacity of Ice. *J. Phys. Chem. C* **2022**, *126*, 8113−8120.
(68) Sherigara, B. S.; Bhat, K. I.; Pinto, I.; Gowda, N. M. M. Oxidation of L-aspartic Acid and L-glutamic Acid by Manganese(III) Ions in Aqueous Sulphuric Acid, Acetic Acid, and Pyrophosphate Media: A Kinetic Study. *Int. J. Chem. Kinet.* **1995**, *27* (7), 675−690.
(69) Bylaska, E. J.; Catalano, J. G.; Mergelsberg, S. T.; Saslow, S. A.; Qafoku, O.; Prange, M. P.; Ilton, E. S. Association of Defects and Zinc in Hematite. *Environ. Sci. Technol.* **2019**, *53* (23), 13687−13694.
(70) Menacherry, S. P. M.; Kim, K.; Lee, W.; Choi, C. H.; Choi, W. Ligand-Specific Dissolution of Iron Oxides in Frozen Solutions. *Environ. Sci. Technol.* **2018**, *52* (23), 13766−13773.
(71) Du, J.; Kim, K.; Min, D. W.; Choi, W. Freeze−Thaw Cycle-Enhanced Transformation of Iodide to Organoiodine Compounds in the Presence of Natural Organic Matter and Fe(III). *Environ. Sci. Technol.* **2022**, *56* (2), 1007−1016.
(72) Malley, P. P. A.; Chakraborty, S.; Kahan, T. F. Physical Characterization of Frozen Saltwater Solutions Using Raman Microscopy. *ACS Earth Sp. Chem.* **2018**, *2* (7), 702−710.
(73) Farnam, Y.; Bentz, D.; Sakulich, A.; Flynn, D.; Weiss, J. Measuring Freeze and Thaw Damage in Mortars Containing Deicing Salt Using a Low-Temperature Longitudinal Guarded Comparative Calorimeter and Acoustic Emission. *Adv. Civil Eng. Mater.* **2014**, *3* (1), 316−337.
(74) Tice, A. R.; Oliphant, J. L.; Nakano, Y.; Jenkins, T. F. *Relationship between the Ice and Unfrozen Water Phases in Frozen Soil as Determined by Pulsed Nuclear Magnetic Resonance and Physical Desorption Data*; CRREL Rep. (US Army Cold Reg. Res. Eng. Lab.), 1982.
(75) Richardson, C. Phase Relationships in Sea Ice as a Function of Temperature. *J. Glaciol.* **1976**, *17* (77), 507−519.
(76) Watanabe, K.; Mizoguchi, M. Amount of Unfrozen Water in Frozen Porous Media Saturated with Solution. *Cold Reg. Sci. Technol.* **2002**, *34* (2), 103−110.
(77) Mel'nichenko, N. A.; Slobodyuk, A. B. Nuclear Magnetic Resonance Study of Sea-Water Freezing Mechanisms: 1. Temperature Dependence of Relative Brine Content in Sea Ice. *J. Glaciol.* **2013**, *59* (216), 711−718.
(78) Vancoppenolle, M.; Madec, G.; Thomas, M.; McDougall, T. J. Thermodynamics of Sea Ice Phase Composition Revisited. *J. Geophys. Res. Ocean.* **2019**, *124* (1), 615−634.
(79) Smit, W. J.; Bakker, H. J. The Surface of Ice Is Like Supercooled Liquid Water. *Angew. Chem.* **2017**, *129* (49), 15746−15750.
(80) Yeşilbaş, M.; Lee, C. C.; Boily, J. F. Ice and Cryosalt Formation in Saline Microporous Clay Gels. *ACS Earth Sp. Chem.* **2018**, *2* (4), 314−319.
(81) Sazaki, G.; Zepeda, S.; Nakatsubo, S.; Yokomine, M.; Furukawa, Y. Quasi-Liquid Layers on Ice Crystal Surfaces Are Made up of Two Different Phases. *Proc. Natl. Acad. Sci. U. S. A.* **2012**, *109* (4), 1052−1055.
(82) Yu, C.; Turner, S.; Huotari, S.; Chen, N.; Shchukarev, A.; Österholm, P.; Lopez-Fernandez, M.; Högfors-Rönnholm, E.; Sachpazidou, V.; Mayanna, S.; Hogmalm, K. J.; Virtasalo, J. J.; Boily, J. F.; Dopson, M.; Åström, M. E. Manganese Cycling and Transport in Boreal Estuaries Impacted by Acidic Mn-Rich Drainage. *Geochim. Cosmochim. Acta* **2024**, *365*, 136−157.

https://doi.org/10.1021/acs.est.4c03850
Environ. Sci. Technol. 2024, 58, 15194−15201